Optimizing the planar structure of (1 1 1) Au/Co/Au trilayers

D P Kumah[1], A Cebollada[1,2], C Clavero[2], J M García-Martín[2], J R Skuza[3], R A Lukaszew[3] and R Clarke[1]

[1] Applied Physics Program and FOCUS Center, University of Michigan, 450 Church St., Ann Arbor, MI 48109-1040, USA

[2] Instituto de Microelectrónica de Madrid-IMM (CNM-CSIC), Isaac Newton 8-PTM, 28760 Tres Cantos, Madrid, Spain

[3] Physics and Astronomy Department, University of Toledo, 2801 W. Bancroft St., Mailstop 111, Toledo, OH 43606, USA

E-mail: dkumah@umich.edu

Abstract
Au/Co/Au trilayers are interesting for a range of applications which exploit their unusual optical and electronic transport behaviour in a magnetic field. Here we present a comprehensive structural and morphological study of a series of trilayers with 0–7 nm Co layer thickness fabricated on glass by ultrahigh vacuum vapour deposition. We use a combination of *in situ* electron diffraction, atomic force microscopy and x-ray scattering to determine the optimum deposition conditions for highly textured, flat and continuous layered structures. The 16 nm Au-on-glass buffer layer, deposited at ambient temperature, is found to develop a smooth (1 1 1) texture on annealing at 350 °C for 10 min. Subsequent growth of the Co layer at 150 °C produces a (1 1 1) textured film with lateral grain size of ~150 nm in the 7 nm-thick Co layer. A simultaneous in-plane and out-of-plane Co lattice expansion is observed for the thinnest Co layers, converging to bulk values for the thickest films. The roughness of the Co layer is similar to that of the Au buffer layer, indicative of conformal growth. The 6 nm Au capping layer smoothens the trilayer surface, resulting in a surface roughness independent of the Co layer thickness.

1. Introduction

The control of crystalline and morphological quality in layered magnetic nanostructures is a key factor for their technological applications as sensors and memory elements. Relevant properties, which include magnetic anisotropies (specifically those of interfacial origin), magneto-optical (MO) activity, interlayer exchange couplings and magneto-transport phenomena, depend sensitively on the thickness of the constituent layers as well as the quality of their interfaces [1]. Recently, there have been interesting developments in this kind of multilayer system exploiting the simultaneous presence of surface plasmon resonances in the noble metal (Au) and the MO activity of the magnetic layer (Co, Cr, etc); this opens new avenues for the development of novel sensing devices [2].

Of special interest in this context is the Au–Co system [3–5], where various multilayered structures were shown to serve as model systems exhibiting unusual magnetic properties. In this case the nature of the crystalline structure, especially at interfaces, played a key role in understanding a variety of magnetic properties, in particular interface anisotropy and giant magneto-resistance (GMR) [6, 7].

The growth of (1 1 1) textured Au layers, and Au/Co/Au trilayers, has long been studied with different scientific goals in mind. For example, Croce *et al* [8, 9] and Chavineau *et al* [10] pioneered the development of the (1 1 1) texture upon annealing Au thin films deposited on amorphous substrates. The growth and study of Au/Co/Au trilayers became of interest during the 1980s and 1990s due to the observation of interfacial magnetic anisotropies, giant magneto-resistance and novel MO phenomena. Among these reports are several works that

concentrated on fundamental magnetic properties [11, 12], the crystalline structure [13, 14] and the interface roughness and its dependence on Co layer thickness [15] in (1 1 1) textured Au/Co/Au trilayers deposited on glass.

Even though several such studies have been published on the growth and structural characterization of specific Au/Co/Au structures, a systematic combined *ex situ* and *in situ* characterization as a function of Co thickness, with the goal of optimizing the planar structure, is still missing. In this paper we present new results on the growth, morphology and crystalline structure of Au/Co/Au trilayers deposited on amorphous glass substrates, where the Co layer thickness has been systematically varied. In our studies we use an initial 16 nm Au buffer layer, which is required to provide an atomically smooth interface and a crystallographic basis on which the ferromagnetic layer (Co) can be grown epitaxially. Finally, a top 6 nm Au layer protects the ferromagnet from oxidation. We varied the Co layer thickness systematically between 0 and 7 nm, and for each sample we characterized the morphology and crystallinity using a combination of real-space and reciprocal-space techniques.

2. Experimental details

The samples were grown in a molecular beam epitaxy (MBE) system with an ultrahigh vacuum (UHV) base pressure of 10^{-10} Torr. Au was deposited by evaporation from an effusion cell and Co was evapourated from an e-beam hearth, with 0.16 and 0.30 nm min^{-1} deposition rates, respectively. The structure and morphology of the samples were studied *in situ* by reflection high energy electron diffraction (RHEED) and *ex situ* by atomic force microscopy (AFM), x-ray diffraction (XRD) and small angle x-ray reflectivity (SAXRR). The substrates on which the films were deposited are standard glass microscope slides ultrasonically cleaned in successive baths of trichloroethylene, acetone and methanol. Before deposition the substrates were outgassed overnight at 200 °C and annealed at 600 °C for 1 h in UHV. The purpose of this annealing step is to promote further planarization of the substrate surface prior to Au deposition. Higher annealing temperatures were avoided as these caused melting of the substrate.

After cooling down the substrate to room temperature (RT) from the annealing temperature (600 °C), a 16 nm Au buffer layer is grown at RT. This buffer layer is then annealed in UHV at 350 °C for 10 min, developing a (1 1 1) texture as evidenced by the appearance of a characteristic streak RHEED pattern independent of the azimuthal angle of the incident electron beam. The buffer layer annealing temperature, though higher than annealing temperatures previously reported in the literature for similar systems, is found to be optimum, maintaining a compromise between surface layer flatness, continuity and crystallinity: lower annealing temperatures produce smaller crystallite sizes and higher annealing temperatures result in the loss of layer continuity by inducing the formation of 3D aggregates. The Au layer is further annealed for an additional 20 min (total of 30 min at 350 °C) to ensure optimum improvement of the crystallinity, even though there is no noticeable change in the RHEED pattern with further annealing after the first 10 min,

as discussed below. The substrate with the Au buffer layer is then cooled down to 150 °C for deposition of Co.

We prepared a series of samples with constant thickness for the Au buffer (16 nm) and Co thickness varying between 0 and 7 nm. The as-deposited Co film exhibits a similar RHEED pattern to that of the Au and corresponds to either the hcp(0 0 0 1) or fcc(1 1 1) stacking order. The crystallographic structure of Co was difficult to determine unequivocally with RHEED since the in-plane lattice spacing of both the hcp and fcc Co are practically the same. Previous x-ray diffraction measurements on Au–Co multilayer structures [4] have revealed hcp stacking in the Co layers. The samples are then cooled down to RT to deposit a Au capping layer $\sim$ 6 nm thick, which also exhibits a similar Au(1 1 1) RHEED pattern, except with broader diffraction streaks. As a reference, one of the samples is grown following exactly the same described steps, but with no Co, i.e. a layer of Au was deposited on glass at RT and annealed at 350 °C followed by the final Au capping layer.

3. Results and discussion

3.1. RHEED measurements

RHEED measurements were recorded *in situ* with a 14.3 keV RHEED gun. In figure 1 we show the evolution of the RHEED pattern during deposition (figure 1(*a*)) and for various times during annealing of the Au buffer layer (figures 1(*b*)–1(*f*)). Figure 1(*g*) shows the RHEED pattern obtained after deposition of 0.3 nm of Co at 150 °C and figure 1(*h*) after the deposition of the subsequent Au capping layer. The ring-like pattern characteristic of a polycrystalline structure is observed in the as-grown Au buffer (figure 1(*a*)). Annealing this buffer layer at 350 °C induces a structural change evidenced by the appearance of well-defined diffraction streaks. At first, these streaks coexist with the rings, then increase in intensity; finally, after 10 minutes of annealing (figure 1(*f*)), the streaks are the only observable features in the RHEED pattern. The Co and Au capping layers exhibit similar RHEED patterns (figures 1(*g*) and 1(*h*)), also independent of the azimuthal orientation of the incident electron beam, and are indicative of the fcc (1 1 1)Au (or close packing, in the case of Co) texture.

The RHEED streaks from the Au buffer layer narrow considerably between 4 and 6 min of annealing, widening slightly and stabilizing in width with further annealing. This indicates an initial smoothing of the surface during the first stages of annealing followed by mild roughening as the annealing proceeds. Restricting the annealing time thus ensures a stable surface for that specific annealing temperature. The RHEED pattern corresponding to the Co layer grown on top of this annealed Au surface exhibits wider streaks, indicative of a Co layer with a somewhat reduced crystalline coherence compared with that of the Au buffer. The Au capping layer seems to revert to the high degree of crystallinity of the Au buffer layer, as evidenced by the narrowing of the streaks compared with the Co layer, with streak spacings equivalent to those observed for the Au buffer layer.

The in-plane lattice spacing can be determined from the separation of the RHEED diffraction streaks. The in-plane lattice spacings were extracted for Co thicknesses of 0.3, 0.8, 0.9, 2.7 and 4.7 nm. The results are presented in figure 2 and
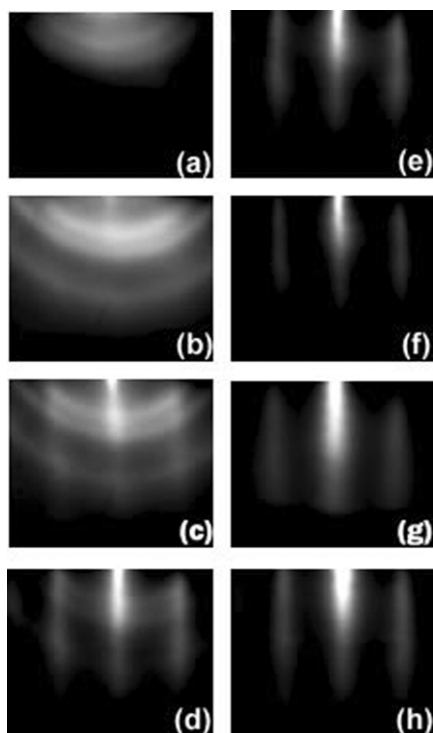
Figure 1. Evolution of the surface structure during the different stages of growth and annealing probed by RHEED: (*a*) 16 nm Au/glass; (*b*)–(*f*) 16 nm Au/glass annealed, respectively, for 2 min, 4 min, 6 min, 8 min and 10 min at 350 °C; (*g*) 0.3 nm Co/16 nm Au/glass; (*h*) 6 nm Au/0.3 nm Co/16 nm Au/glass. See text for deposition conditions. The RHEED streaks in (*c*)–(*h*) correspond to the (1 1 0) diffraction zone.
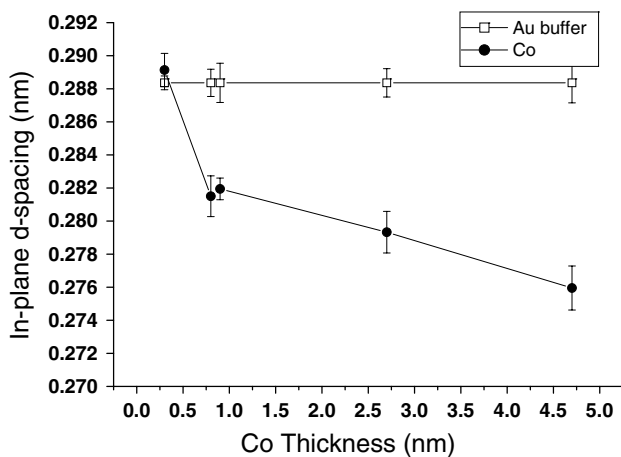

Figure 2. In-plane lattice spacings for the Au buffer layer and Co spacer determined from RHEED measurements of a set of 6 nm Au/t Co/16 nm Au/glass structures where $t = 0.3, 0.8, 0.9, 2.7$ and 4.7 nm.

compared with those for the Au buffer layer. The observed in-plane lattice spacing for Au is constant for all the samples and corresponds to the (1 1 0) spacing for bulk fcc Au ($d_{110} = 0.288\,36$ nm). The literature value for the bulk in-plane close-packed spacing for Co is 0.250 7 nm which corresponds to a 13% lattice mismatch with respect to the Au film. For the thin Co films (t Co < 0.8 nm), the observed Co spacing is very close to that of Au, indicative of the presence of coherent
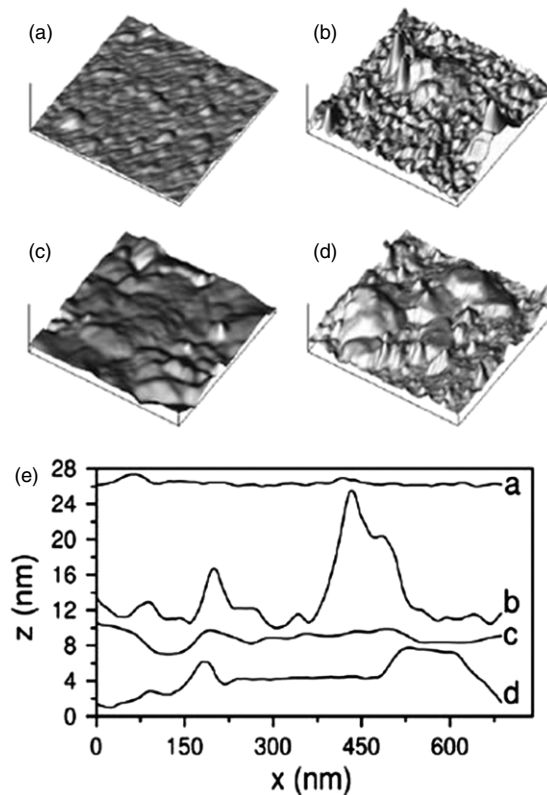

Figure 3. AFM data probing morphology and surface roughness: (*a*) image of bare annealed glass substrate; (*b*)–(*d*) images showing the influence of different thermal treatments on the surface morphology of 6 nm Au / 2.7 nm Co / 16 nm Au /glass. The AFM images have the same scale (20 nm vertical and 700 nm lateral); (*e*) characteristic profiles across images (*a*)–(*d*).

interfaces with a large tensile strain introduced as a result of the lattice mismatch. A linear relaxation of the Co in-plane lattice spacing towards the bulk value is observed as the Co thickness increases. At 4.7 nm, the Co film is still not completely relaxed, being expanded by about 8%. Previous works have shown that annealing the Co film can induce complete relaxation of the bulk value for films as thin as 1.3 nm due to loss of interface coherence [16], which indicates that in the present work at least partial interface coherency persists with increasing Co thickness.

3.2. Atomic force microscopy measurements

The morphology of the samples is studied by combined AFM and SAXRR measurements. AFM is especially useful in helping determine the optimum deposition and annealing temperatures, i.e. the conditions giving rise to smoother surfaces and interfaces for the trilayer samples used in this study. First, in figure 3(*a*) we show the AFM image of the initial surface upon which all the structures are deposited, i.e. a glass substrate, prepared as described earlier. The surface exhibits an rms roughness of 0.3 nm calculated from the height histograms of 0.7 μm × 0.7 μm AFM images and represented as the FWHM of the peak centred at the average height. In figures 3(*b*)–(*d*) we show AFM images for three 6 nm Au/2.7 nm Co/16 nm Au/glass trilayers grown with different thermal treatments. In figure 3(*b*), we show the morphology
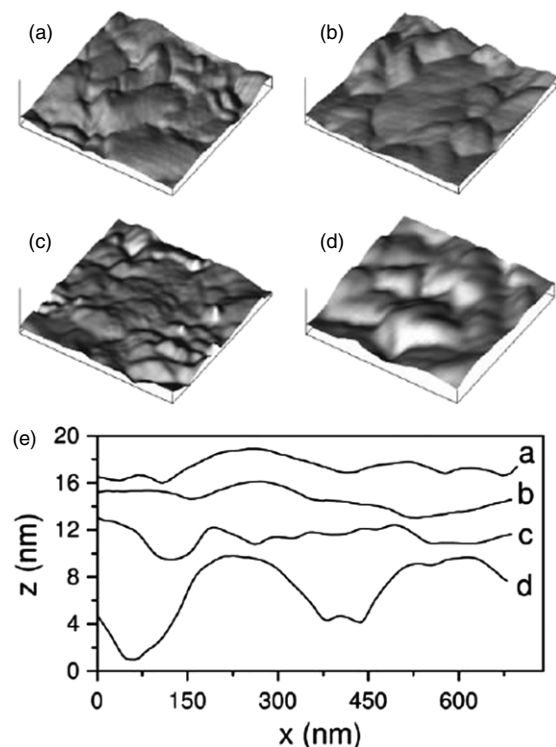
Figure 4. AFM images of samples prepared with optimized thermal treatment at different Co film thicknesses. (*a*)–(*d*): AFM images of 6 nm Au/ *t* Co /16 nm Au /glass samples with *t* = 0 nm, 0.5 nm, 2.7 nm and 7.0 nm, respectively. Image scale: 20 nm vertical, 700 nm lateral, (*e*) characteristic profiles of AFM images (*a*)–(*d*).
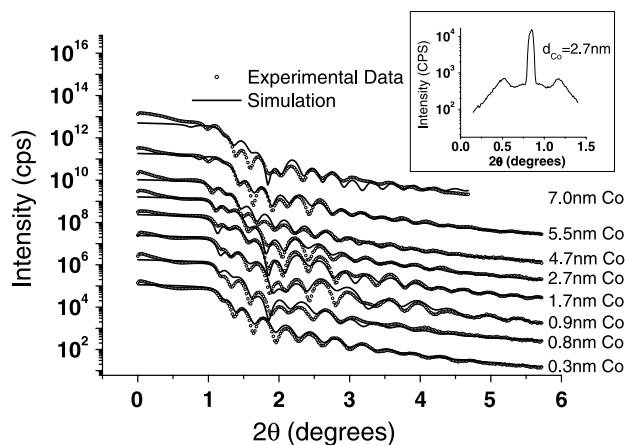

Figure 5. Low angle x-ray reflectivity curves for the complete set of 6 nm Au/*t* Co/16 nm Au/glass structures, with *t* between 0.3 and 7.0 nm. Inset: rocking curve for *t* = 2.7 nm sample.

of a trilayer where the three layers were grown at RT with no annealing. Figure 3(*c*) shows the AFM image corresponding to a trilayer following the thermal treatment selected for the whole series of samples (Au buffer grown at RT and annealed at 350 °C for 30 min followed by Co deposition at 150 °C and Au capping layer grown at RT). In figure 3(*d*) we show the AFM image of a sample equivalent to that shown in figure 3(*c*), but with the Au capping layer deposited at 150 °C. Finally, the corresponding characteristic line profiles of the substrate and the trilayers are shown in figure 3(*e*).

As can be seen, deposition of the trilayers in all cases leads to an increase in the overall roughness with respect to the initial substrate surface. The trilayer deposited at RT shows a strong lateral corrugation with hills and valleys of several nanometres amplitude. On the other hand, the trilayer shown in figure 3(*c*) exhibits a much smoother surface with a roughness of 1.2 nm. Finally, the trilayer with the cap grown at 150 °C shows terraces a few nm high, due to the thermally enhanced diffusion of the Au atoms that promotes the formation of 3D structures. In fact, the height histogram of this sample (not shown) exhibited several maxima corresponding to the different height values of these terraces. From these AFM comparisons we are able to confirm that the selected thermal process leads to the smoothest surfaces.

Figure 4 shows the morphology of representative trilayers grown under the optimized thermal treatment for Co thicknesses of 0, 0.5, 2.7 and 7.0 nm. Figure 4(*a*) shows an AFM image for 0 nm Co, i.e. a sample with Au buffer layer and Au capping layer but without any Co film in-between.

Figures 4(*b*)–(*d*) show AFM images of trilayers with Co layer thicknesses of 0.5 nm, 2.7 nm and 7 nm, respectively. The corresponding characteristic line profiles are shown in figure 4(*e*) and labelled accordingly. We can conclude that the overall roughness increases with Co thickness, being 1 nm for 0 nm and 0.5 nm of Co and increasing to 1.2 nm and 3.3 nm for 2.7 nm and 7.0 nm of Co, respectively.

3.3. Small angle x-ray reflection measurements

We performed SAXRR measurements using a Cu-Kα source ($\lambda = 0.154\,506$ nm) with a graphite monochromator. Film thickness and roughness are obtained by fitting the experimental data [17]. The fitting parameters are the thickness and roughness of the Au and Co layers. The nominal thickness measurements from the calibrated quartz balance and estimates based on the deposition rates are used as the initial fitting parameters. We determine the final thickness and roughness values by iteratively varying the parameters to obtain the best fit.

In figure 5 we show SAXRR measurements on our samples together with the corresponding simulated fits. The fit is very good, although some systematic deviations are observed for 2θ values below the critical angle ($<0.5°$), probably due to spill-over of the relatively wide incident x-ray beam. Nominal and extracted Au and Co thicknesses are in good agreement. The inset of figure 5 shows the rocking curve measured at a reflection maximum for the 2.7 nm Co sample. Yoneda wings, characteristic of relatively smooth (i.e. specular) surfaces with lateral surface features, are clearly observed. In figure 6 we show the extracted Co and Au buffer and capping layer roughness as a function of the Co layer thickness. We can clearly observe that both the Au buffer layer and the Co layers yield similar roughness values (between 0.7 and 1.5 nm) for all Co thicknesses, indicative of conformal growth of the Co on the buffer layer. On the other hand, the Au capping layer presents much lower roughness values (between 0.2 and 0.3 nm), indicating a planarization of the surface, as observed in the case of Au/Fe/Au previously studied using soft x-ray reflectivity [18].

The lower Co and Au cap roughness obtained for samples with very thin Co layers must be considered with care, since
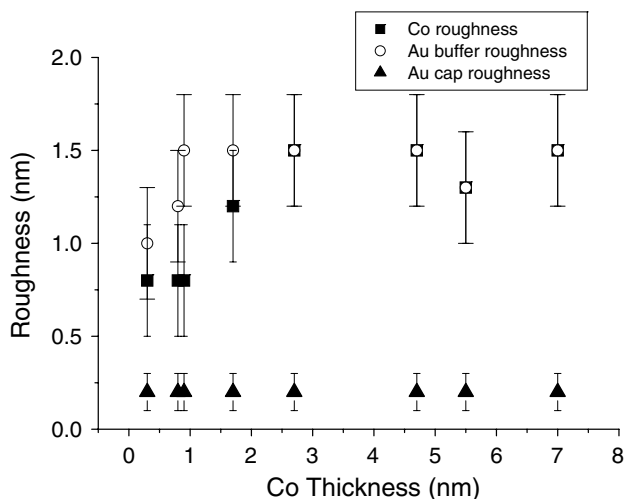
Figure 6. Roughness of the Au buffer, Au capping layer and Co spacer for 6 nm Au / *t* Co /16 nm Au /glass structures as a function of the thickness of the Co spacer determined from fitting SAXRR measurements.

Figure 7. High angle x-ray diffraction scans for the 6 nm Au / *t* Co /16 nm Au /glass structures, with *t* between 0 and 7.0 nm. The fits are obtained by assuming a kinematic diffraction model for x-ray scattering. The plots are displayed as a stack for clarity.

for the thinnest Co layers, with thickness on the order of the roughness of the Au layer underneath, the continuous nature of the Co layer is not guaranteed, and therefore the applied formalism would not be valid in this case. On the other hand, we note that different roughness values are obtained from SAXRR and AFM measurements (only the Au capping layer roughness is measured in AFM), with smaller values obtained from the SAXRR fits. Here it is important to note that different formalisms are used to extract these values from each technique, and more important, the lateral extent probed with the different techniques are not equivalent and thus the extracted numeric values may not coincide. In the case of AFM, the lateral length scale is that of the whole scanned area (700 nm × 700 nm), whereas for SAXRR, it is the x-ray lateral coherence length (<100 nm). This could explain the smaller values of roughness obtained with SAXRR compared wiht those measured by AFM. Similar differences have been noted in previous studies of roughness and growth scaling exponents of other thin film materials and are generally ascribed to the different lateral length scales of the height–height correlation function probed by x-ray reflectivity and scanning probe techniques [16,19–22]. In fact, one can try to 'simulate' the deduction of the SAXRR roughness from the AFM images by dividing such images into 100 nm × 100 nm areas, evaluating the rms roughness in each one and finally calculating the average value. The average roughness values obtained with this procedure are 0.3 and 0.8 nm for the samples with 0 and 7 nm of Co, which are now closer to the values depicted in figure 6 for the Au cap.

3.4. X-ray diffraction

Figure 7 shows high-angle XRD symmetric 2θ–ω scans measured for all the samples using a Cu-Kα source and a Panalytic X'Pert PRO diffractometer fitted with a channel-cut Ge(220) monochromator and an X-Celerator Real Time Multiple Strip array detector. The vertical dashed lines shown in the plot indicate the positions for bulk fcc Au(1 1 1), hcp Co(00.1) and fcc Co(1 1 1). In all the cases
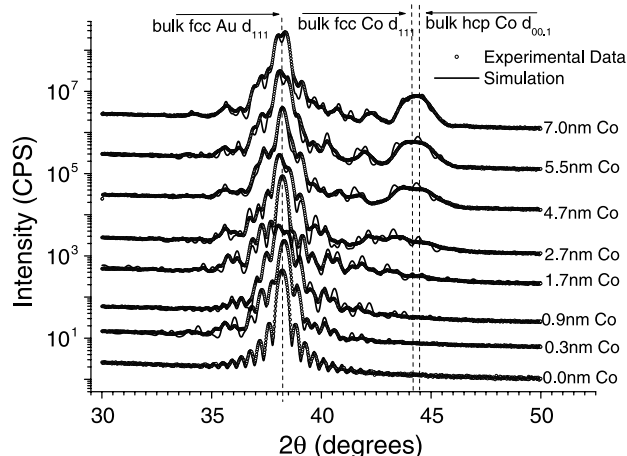
the Au(1 1 1) reflection is clearly observed together with Pendellösung interference fringes which are indicative of the good interface coherence and high crystalline quality along the surface normal of the specimens. The presence of the Co layer modulates the intensity of these interference fringes. The intensity of the fringe features related primarily to the Co layer decreases with Co film thickness and fades out around $t_{Co} = 1.7$ nm. The Co-related envelope in the thicker samples is broadened, indicative of a gradual relaxation of the bulk lattice spacing.

The individual layer thicknesses and the out-of-plane interatomic spacings can be extracted by fitting the experimental XRD data assuming a kinematical one-dimensional step model [14, 22]. The total scattering amplitude from the multilayer is obtained by summing up the contributions from the individual monolayers in the structure. The variables in the fitting procedure are the interplanar spacings for the capping Au layer (d_{AuCap}) and the Co spacer (d_{Co}). We assume a bulk d_{111}(Au) spacing for the 16 nm Au buffer layer and allow d_{Co} and d_{AuCap} to vary to obtain the best fit to the experimental data. To model roughness, we assume a finite interface width between the layers with a gradient in the lattice parameter in this region. The gradient is also allowed to vary to obtain the best fit to the experimental data. It is however difficult to obtain reliable lattice values for the very thin Co samples ($t_{Co} < 0.5$ nm) because the roughness of the Au buffer is on the order of the thickness of Co. As shown in figure 8, for the $t_{Co} = 0.3$ nm sample, the out-of-plane d-spacing for Co, which gives the best fit for our data, is 0.212 nm which represents a 4% out-of-plane expansion for the first 2 layers of Co. This is the opposite of what might be expected based on the in-plane tensile strain of Co measured by RHEED, i.e. the large in-plane expansion observed from RHEED should result in an out-of-plane contraction of the Co unit cell. The next 2–3 atomic layers of Co are expanded by about 2%. Subsequent layers of Co are found to relax to the bulk hcp $d_{00.1}$(Co) value of 0.203 4 nm (or bulk fcc d_{111}(Co) = 0.204 7 nm). This observation is consistent with previous results from RHEED studies [15] and electron diffraction studies of Au/Co multilayers by Mliki *et al* [14],
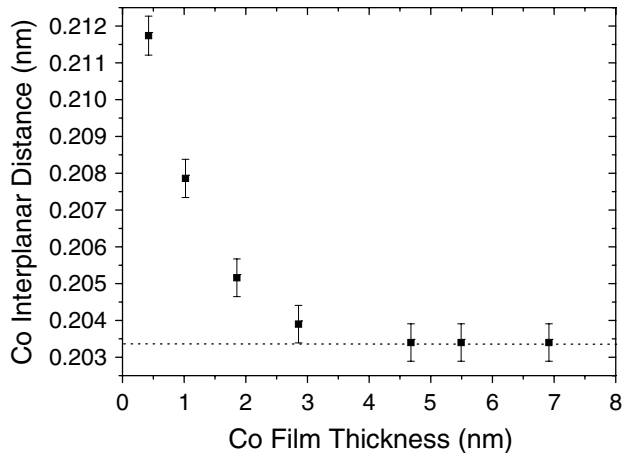
Figure 8. Evolution of the Co out-of-plane interplanar spacing as a function of Co thickness determined by fitting the XRD results for 6 nm Au / *t* Co /16 nm Au /glass samples with *t* between 0 and 7 nm. The dashed line indicates the position of the bulk hcp Co (00.1) spacing.

who argue that the large lattice mismatch leads to a volume expansion and consequent distortion of the Co unit cell for the first few monolayers. Lee *et al* [4] also concluded that the large mismatch between Au and Co is taken up by misfit dislocations between the in-plane epitaxially oriented domains. However, it is also possible that the observed expanded lattice spacing is due to intermixing at the interface resulting from roughness. Note that the observed roughness from our SAXRR measurements presented above is on the order of the Co thickness, for Co thicknesses less than 0.9 nm. For the sample with no Co film, the exact bulk Au lattice spacing is experimentally obtained for both the buffer and the capping Au layer.

4. Conclusions

We have studied the Co thickness dependence of the interface roughness and interplanar spacings in Au/Co/Au structures grown on glass substrates. We have devised a thermal treatment which optimizes the surface smoothness and crystallinity using structural and morphological characterizations from x-ray, AFM and RHEED studies. The Au is polycrystalline and oriented in the (1 1 1) direction. The Co grows epitaxially on the (1 1 1) fcc Au layer with excellent interface coherence as evidenced by RHEED and XRD results. We observe from the RHEED and XRD data, a volume expansion for the Co film. An in-plane expansion of about 13% is seen for the first 4 monolayers of Co, relaxing isotropically to about 8% after 20 monolayers of Co are deposited. The out-of-plane expansion of the Co lattice is determined to be about 4% for the first 2 atomic layers, followed by a relaxation to the bulk lattice spacing after 2–3 more atomic layers of Co. SAXRR was used to determine the roughness at the interfaces in the multi-layer as a function of the Co thickness. We conclude that the

Co roughness is independent of the Co thickness and dependent on the roughness of the Au buffer layer for Co thicknesses up to 7 nm. The deposition conditions identified in this study will be beneficial for preparing optimized samples for MO and magneto-plasmonic applications.

References

[1] Schuller I K, Kim S and Leighton C 1999 *J. Magn. Magn. Mater.* **200** 571
[2] Sepúlveda B, Calle A, Lechuga L M and Armelles G 2006 *Opt. Lett.* **31** 1085
[3] Lee C H, He H, Lamelas F J, Vavra W, Uher C and Clarke R 1989 *Phys. Rev.* B **42** 1066
[4] Lee C, He H, Lamelas F, Vavra W, Uher C and Clarke R 1989 *Phys. Rev. Lett.* **62** 653
[5] Vavra W, Lee C H, Lamelas F J, He H, Clarke R and Uher C 1990 *Phys. Rev.* B **42** 4889
[6] Stavroyiannis S, Christides C, Niarchos D, Kehagias Th, Komninou Ph and Karakostas Th 1998 *J. Appl. Phys.* **84** 6221
[7] Wellock K, Caro J and Hickey B 1999 *J. Magn. Magn. Mater.* **198–199** 27
[8] Croce P, Devant G, Gandais M and Marraud A 1961 *Rev. Opt.* **40** 555
[9] Croce P, Devant G, Gandais M and Marraud A 1962 *Acta Crystallogr.* **15** 424
[10] Chavineau J, Croce P, Devant G and Verhaeghe M 1969 *J. Vac. Sci. Technol.* **6** 776
[11] Chappert C, Renard D, Beauvillain P and Renard J 1985 *J. Physique Lett. (Paris)* **46** L59
[12] Chappert C, Renard D, Beauvillain P, Renard J and Seiden J 1986 *J. Magn. Magn. Mater.* **54–57** 795
[13] Renard D and Nihoul G 1987 *Phil. Mag.* B **55** 75
[14] Mliki N, Abdelmoula K, Nihoul G, Marlière C and Renard D 1993 *Thin Solid Films* **224** 14
[15] Marlière C, Renard D and Chauvineau J 1991 *Thin Solid Films* **201** 317
[16] Wawro A, Baczewski L, Pankowski P, Kisielewski M, Sveklo I and Maziewski A 2002 *Thin Solid Films* **412** 34
[17] Bridou F and Pardo B A 1990 *J. Opt. (Paris)* **21** 183
[18] Marlière C, Chauvineau J P and Renard D 1990 *Thin Solid Films* **189** 359
[19] Thomson G, Palasantzas G, Feng Y P, Sinha S K and Krim J 1994 *Phys. Rev.* B **49** 4902
[20] Wang J, Li G, Yang P, Cui M, Jiang X, Dong B and Liu H 1998 *Europhys. Lett.* **42** 283
[21] Stone V W, Jonas A M, Nysten B and Legras R 1999 *Phys. Rev.* B **60** 5883
[22] Palasantzas G 1993 *Phys. Rev.* B **48** 14472
[23] Segmuller A and Blakeslee A E 1973 *J. Appl. Crystallogr.* **6** 19